

Study on the Improvement of TOPAZ-II system by Using a Heat Pipe Radiator

Wenwen Zhang, Wenxi Tian, Suizheng Qiu*, and Guanghui Su
School of Energy and Power Engineering in Xi'an Jiaotong University
No.28 Xianning West Road, Xi'an 710049, Shaanxi, China
zhang.wen.wen.1@stu.xjtu.edu.cn; wxtian@mail.xjtu.edu.cn;
szqiu@mail.xjtu.edu.cn; ghsu@mail.xjtu.edu.cn

ABSTRACT

The former Soviet Union TOPAZ-II reactor system uses a coolant tube radiator which has single point failure problem. With no changing of the other parts of the system, a heat pipe type radiator is preliminarily designed to replace the coolant tube radiator and increase the reliability of the space system. According to the requirement of heat dissipation and the coolant operating temperature, the liquid-metal heat pipes with potassium is selected. Its structure materials are selected and the parameters are designed in detail. The structure of heat pipe radiator, the layout of the heat pipes and the fin are also designed. The central heat pipe steam region is modeled by one-dimensional flow equations. The heat transfer of the heat pipe wall and wick are solved by the finite element method while that of the fin using finite difference method. The steady state results of the radiator under nominal conditions are obtained by the coupling calculation of heat pipes and the transport duct. The characters of the heat pipe radiator is compared with that of coolant tube radiator. The results show that the heat pipe radiator designed in this paper meets the requirements of the TOPAZ-II system under the normal conditions and has a ideal margin. The isothermal and safety of heat pipe radiator are better than that of coolant tube radiator.

KEYWORDS

TOPAZ-II; heat pipe design; radiator; numerical simulation

1. INTRODUCTION

Future exploitation and exploration of space that will demand large power sources, including high power communications and remote sensing satellites, deep space exploration, extraterrestrial manufacturing, manned missions to Mars, and colonization of the Moon. Many of these tasks will take place in harsh environments where solar power is limited, intermittent, or unavailable. Nuclear power can serve as a compact durable energy source that is capable of long-term operation in space. The Russian TOPAZ-II system is the most technologically advanced thermionic system ever built^[1]. The system provides power using thermionic energy conversion and rejects the waste heat by a coolant tube radiator, which consists of 78 coolant tubes^[2]. As shown in Fig.1, the radiator is shaped as a truncated cone, whose bases are formed by upper and lower headers. The coolant tube radiator has a simple structure and good radiation performance, but the possibility of a single point failure exists, which means a micrometeoroid puncture of a cooling-fluid carrying tube would cause eventual loss of cooling fluid, thus leading to failure of the radiator. And for the space reactor system, once this accident occurs, the entire system will failure for no possibility of repair. In contrast, space radiators composed of a large number of heat pipes would be

relatively immune to puncture from micrometeoroids or small space debris because loss of an individual heat pipe, whose function is completely independent of that of its neighbors, would result only in the loss of that small fraction of total radiating area. Thus, overall radiator reliability can be significantly enhanced.

The heat pipe radiator provides redundancy without failures propagation and single-point failures. The failure of one or several heat pipes will not affect the whole system's operation. In the modern space devices, the heat pipe has been widely applied. Liquid-metal heat pipes are considered for thermal energy transport in many high temperature and high power density space power and energy systems. Several space reactor power system concepts have been developed with liquid metal heat pipes for the waste heat rejection or the passive and transport of the fission power generated in reactor to the energy conversion subsystem, such as the American SPACE-R thermionic reactor system^[3], SP-100 thermocouple reactor system^[4], SCoRe system^[5], SAIRS system^[6].

Based on the design of other space power system radiators, a alkali metal heat pipe radiator is designed to improve the reliability of the TOPAZ-II system. Meanwhile, using the numerical simulation method, the designed heat pipe radiator is analyzed under steady state.

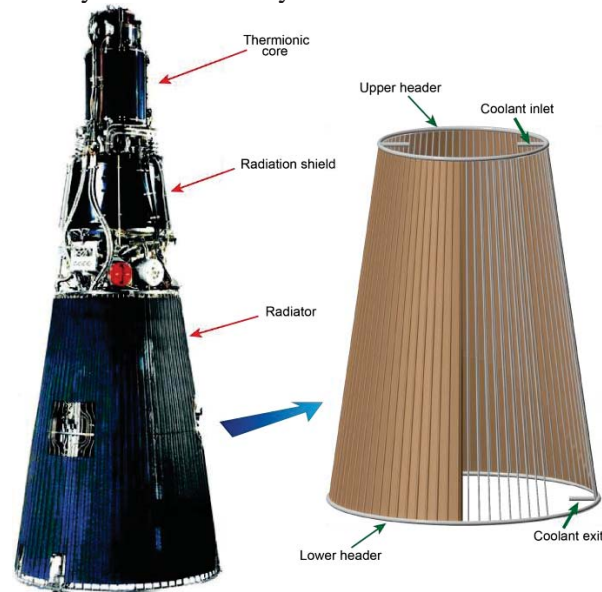


Fig. 1 Schematics of TOPAZ-II power system and the coolant tube radiator

2. THEORETICAL MODELS

2.1. HEAT PIPE MATERIAL SELECTION

There are three basic components of a heat pipe, the working fluid, the wick or capillary structure and the shell. In the selection of a suitable combination of the three parts, inevitably a number of conflicting factors may arise. For the high temperature heat pipe, alkali metal is generally used as the working fluid, including lithium, sodium, potassium and rubidium. The coolant of TOPAZ-II system works in the range of 700K-900K, so the potassium is selected. The material selection for the wick and wall of alkali-metal heat pipes depends on the operating temperature and pressure, type of working fluid. With reference to the design of similar radiator, the Inconel is the preliminary selection as the material of the pipe shell and the steel wire mesh as the heat pipe wick. The integral graphite-carbon composite fin(C-C fin) is applied in this paper for its higher thermal conductivity and lower density.

2.2. OPERATION LIMITS OF HEAT PIPES

Although the heat pipe has an excellent performance of heat transfer, a series of limits exist. The operation limits of a heat pipe, in the order of increasing power throughout and temperature, are the viscous, sonic wicking or capillary, entrainment and boiling. These limits are affected by the size and shape of heat pipe, working fluid, temperature and other related parameters, and they are important basics for the design and verification of the heat pipe^[7].

The heat pipe has a constant diameter and the steam accelerates due to the vapor mass injection in the evaporation section, and decelerates for the vapor condensation in the condensation section. When the steam achieves sonic velocity in the evaporation section, critical flow condition occurs. The change in the condensation section will not upriver to the evaporation section and the temperature of condensation section has no effect on the evaporation section. The heat pipe meets the sonic limit in this situation. The sonic limit, is always encountered at low temperatures, should be avoided. The heat pipe sonic limit can be expressed as:

$$Q_{s,max} = \frac{A_v \rho_o h_{fg} M_v \sqrt{\gamma_v R_v T_o} \left(1 + \frac{\gamma_v - 1}{2} M_v^2\right)^{1/2}}{1 + \gamma_v M_v^2} \quad (1)$$

$$d_v = \frac{20 Q_{s,max}}{\pi \rho_o h_{fg} \sqrt{\gamma_v R_v T_o}} \quad (2)$$

where, A_v is the cross sectional area of vapor region, h_{fg} is the latent heat of potassium, M_v is the molecular weight of the vapor, γ_v is the vapor specific heat ratio, R_v is the perfect gas constant, T_o is potassium heat pipe operating temperature.

The capillary limit is encountered when the net capillary pressure head is less than the combined pressure losses of the liquid flow in the wick and of the counter-current vapor flow in the heat pipe. The capillary pressure head for circulating the heat pipes working fluid increases with increasing the liquid surface tension and decreasing radius of curvature of the liquid-vapor meniscus in the surface pores in the wick. In order for the heat pipe to operate, Equation (3) must be satisfied, namely

$$\Delta p_{c,max} \geq \Delta p_l + \Delta p_v + \Delta p_g \quad (3)$$

When the capillary heat transfer limit occurs, the maximum theoretical capillary pressure can be expressed as:

$$\Delta p_{c,max} = Q_{c,max} (F_l + F_v) + \Delta p_g \quad (4)$$

where, F_l is the friction coefficient of liquid, F_v is the friction coefficient of vapor, Δp_g is the gravitational pressure drop which will be zero in space in the weightlessness conditions.

In a heat pipe the vapor flows from the evaporator to the condenser and the liquid is returned by the wick structure. At the interface between the wick and the vapor the latter will exert a shear force on the liquid in the wick. The magnitude of the shear force will depend on the vapor properties and velocity and its action will be to entrain droplets of liquid and transport them to the condenser end. This tendency to

entrainment is resisted by the surface tension in the liquid. Entrainment will prevent the heat pipe operating and represents one limit to performance.

The following equation gives the entrainment limiting flux:

$$Q_{e,\max} = A_v h_{fg} \left(\frac{\rho_v \sigma}{2r_{hs}} \right)^{1/2} \quad (5)$$

where, σ is the surface tension of the liquid metal potassium, r_{hs} is the hydraulic radius of capillary wick.

A boiling at the inner surface of the heat pipe wall in the evaporator section is likely when the local liquid superheat exceeds that for incipient nucleate boiling. The ensuing nucleation and growth of vapor bubbles blocks the flow of the liquid in the wick and would cause the heat pipe burn up. The following equation gives the boiling limiting flux:

$$Q_{b,\max} = \frac{2\pi l_e \lambda_{eff} T_v}{h_{fg} \rho_v \ln(r_i / r_v)} \left(\frac{2\sigma}{r_b} - \Delta p_c \right) \quad (6)$$

where, l_e is the length of the evaporator, r_b is the vaporization center radius of bubbles, Δp_c is the maximum capillary pressure, r_i/r_v is the ratio between the heat pipe diameter and the steam cavity diameter, λ_{eff} is the effective thermal conductivity and can be expressed as:

$$\lambda_{eff} = \frac{\lambda_l [(\lambda_l + \lambda_s) - (1 - \varepsilon)(\lambda_l - \lambda_s)]}{[(\lambda_l + \lambda_s) + (1 - \varepsilon)(\lambda_l - \lambda_s)]} \quad (7)$$

2.3. MATHEMATICAL MODELS OF THE HEAT PIPE RADIATOR STEADY ANALYSIS

Based on the design of the radiator of SPACE-R reactor power system, combined with the original TOPAZ-II radiator shape, a truncated cone radiator using the heat pipe is designed, as shown in Fig.2. The pipes are inserted into the transport duct with the staggered arrangement. The transport duct adopts a rectangular cross section.

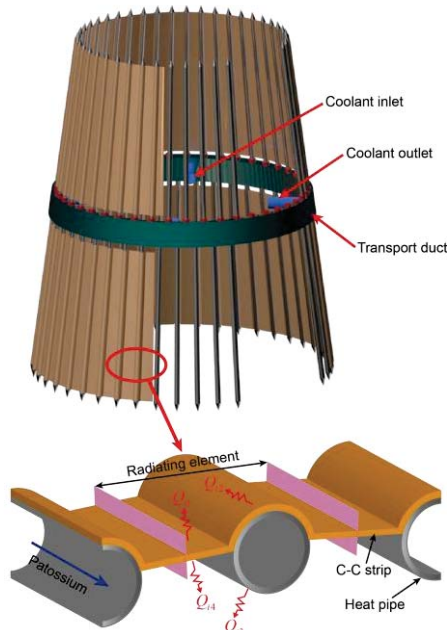


Fig. 2 Design and layout of the heat pipe radiator

2.3.1. HEAT PIPE WALL AND WICK STRUCTURE

Based on the study of the reference^[8], the density of the liquid state sodium is much greater than that of the vapor state, so that the velocity of liquid sodium in the wick structure is very small. Also, the thermal conductivity of liquid sodium is large and the thickness of the wick is very thin. It is then assumed that influence of the liquid flow in the wick is negligible and the pure conduction model is applied in the wick. So, in the pipe wall and wick region, the heat transfer procedure can be modeled by the heat conduction equation in cylindrical coordinate. The governing equation is expressed as follows:

$$\frac{1}{R} \frac{\partial}{\partial R} \left(R \lambda_i \frac{\partial T_i}{\partial R} \right) + \frac{\partial}{\partial Z} \left(\lambda_i \frac{\partial T_i}{\partial Z} \right) = 0, \quad i = 1, 2 \quad (8)$$

where, $i = 1$ and $i = 2$ present the pipe wall and wick structure, respectively.

2.3.2. VAPOR REGION

During the operation of the heat pipe, the vapor will experience free molecular, choked, and continuum flow at various times. The present work just calculates and analyses the steady condition of the heat pipe after startup, so only the continuum stage was modeled. Even though the Reynolds number depends on the geometry of the heat pipe and the actual heat transfer rate, the results cited from the previous study show that the vapor flow in the heat pipe may be assumed laminar. Also, the density of the vapor is very small so that the compressibility should be considered. Thus, compressible, one-dimensional laminar flow in the vapor space is considered. For purpose of formulating the mass, momentum, and energy equations in one-dimensional form, the average velocity is taken. In addition, friction at the liquid-vapor interface, and momentum and energy factors are similarly calculated. Mass, momentum and energy balances in the axial direction are as follows:

$$D \frac{d}{dZ}(\rho V) = \dot{m}_0 \quad (9)$$

$$\frac{dP}{dZ} + \frac{d}{dZ}(M_f \rho V^2) = -\frac{F \rho V^2}{8D} \quad (10)$$

$$D \frac{d}{dZ} \left[\rho V \left(h + \frac{E_f V^2}{2} \right) \right] = \dot{m}_0 \left(h_0 + \frac{V_0^2}{2} \right) \quad (11)$$

A friction factor for the surface is written as

$$F = \frac{8\tau g}{\rho V^2} \quad (12)$$

Momentum and energy factors are expressed as

$$M_f = \frac{1}{DV^2} \int_0^D U^2 dy \quad (13)$$

$$E_f = \frac{1}{DV^3} \int_0^D U^3 dy \quad (14)$$

Based on the mass, momentum and energy balances in the axial direction, the gas state equation and other constitutive equations, the axial gradients for the vapor density, quality, velocity, pressure, and temperature can be derived. The equations are written as follows:

$$\frac{d\rho}{dZ} = -\frac{1}{v^2} \left[(\nu_g - \nu_f) \frac{dX}{dZ} + \frac{\nu_g X}{p} \left(\frac{R_v T}{h_{fg} M} - 1 \right) \frac{dp}{dZ} \right] \quad (15)$$

$$\frac{dX}{dZ} = \frac{v^2}{(\nu_g - \nu_f) V^2} \left\{ \left[-\frac{1}{M_f} + \frac{V^2 X}{p} \frac{\nu_g}{v^2} \left(1 - \frac{R_v T}{h_{fg} M} \right) \right] \frac{dp}{dZ} - \frac{F V^2}{8D v M_f} \right\} - \frac{v^2}{(\nu_g - \nu_f) DV} \frac{2\dot{m}_0}{DV} \quad (16)$$

$$\frac{dV}{dZ} = \frac{v \dot{m}_0}{D} + \frac{V(\nu_g - \nu_f)}{v} \frac{dX}{dy} + \frac{VX}{p} \frac{\nu_g}{v} \left(\frac{R_v T}{h_{fg} M} - 1 \right) \frac{dp}{dZ} \quad (17)$$

$$\frac{dp}{dZ} = \frac{-\frac{M_f}{E_f} \frac{\dot{m}_0}{VD} \left[2h_{fg} + \frac{(\nu_g - \nu_f)}{v} \left(h_0 - h + \frac{E_f V^2}{2} + \frac{V_0^2}{2} \right) \right] - \frac{1}{E_f} \frac{h_{fg}}{v} \frac{F}{8D} - \frac{(\nu_g - \nu_f)}{v^2} \frac{F V^2}{8D}}{\frac{(\nu_g - \nu_f)}{v} + \frac{1}{E_f} \frac{h_{fg}}{V^2} - \frac{M_f}{E_f} \frac{h_{fg} X}{p} \frac{\nu_g}{v^2} \left(1 - \frac{R_v T}{h_{fg} M} \right) - \frac{M_f}{E_f} \frac{(\nu_g - \nu_f)}{v^2} \frac{c_p R_v T^2}{h_{fg} M p}} \quad (18)$$

$$\frac{dT}{dZ} = \frac{R_v T^2}{h_{fg} M p} \frac{dp}{dZ} \quad (19)$$

2.3.3. NUMERICAL METHOD

The governing equations are solved separately for each region and coupling is implemented at the interface. The finite element method(FEM) is employed for the heat pipe shell and wick., and the phase change of the working fluid during the accident is modeled with the equivalent heat capacity method. The Runge-Kutta method is applied to solve the first-order differential nonlinear equations of the vapor zone. Fig.3 shows the two-dimension mesh division of the heat pipe.

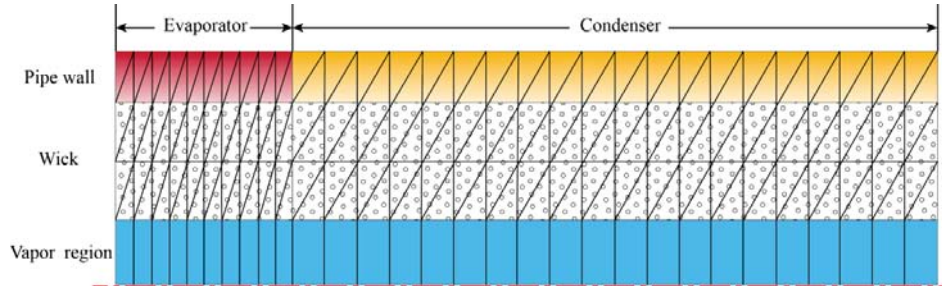


Fig. 3 Finite element mesh for the conduction heat transfer

2.4. MATHEMATICAL MODEL OF THE FIN

The basic mechanism of heat transfer in the space radiator is conduction combined with radiation. A radiating element consists of a heat pipe, the C-C strip welded to it and two half part of the flat fin. For each radiating element, the radiation can also be divided into four parts: heat dissipated from the welded strip, naked part of the heat pipe wall, two surfaces of the flat fin. The radiation of the welded fin and naked part of the heat pipe wall can be estimated by

$$Q_{i1} = f_{wc} \varepsilon_{wc} \sigma \left(\frac{\pi \theta (d + \delta_{fin})}{360} \right) L_i (T_{wci}^4 - T_s^4) \quad (20)$$

$$Q_{i4} = f_{pw} \varepsilon_{pw} \sigma \frac{(360 - \theta) \pi d}{360} L_i (T_{pwi}^4 - T_s^4) \quad (21)$$

where, f_{wc} and f_{pw} are the geometric view factors of the welded strip and the naked pipe, respectively; T_{wci} and T_{pwi} are the temperature of the welded strip and the naked pipe wall associated to the control volume i of the pipe. The T_{wci} is obtained by one-dimension conduction of the welded strip with a radiation boundary of the outer surface.

Since the fin is thin, the temperature distribution within the fin is assumed to be two-dimensional. In order to simplify the modeling, the radiation between the fin and heat pipe is neglected. The energy balance equation for a differential element of the fin is given as:

$$\frac{d^2 T_{fin}}{dx^2} = - \frac{Q_{i2} + Q_{i3}}{dx \cdot \lambda \cdot \delta_{fin} \cdot L_i} = - \frac{(f_{sout} \varepsilon_{sout} + f_{sin} \varepsilon_{sin}) \sigma (T_{fin}^4 - T_s^4)}{\lambda \delta_{fin}} \quad (22)$$

The integration method or the Monte Carlo method can be employed to find the view factors. In this case, the view factors for all parts were calculated by the software MCNP. Considering the symmetry of the fin between the adjacent pipes, just half of it is modeled. The finite difference method(FDM) is used to discretize the Eq.22 and the discrete equations obtained are calculated by Newton iterative method. The

scheme of the fin solution is presented in Fig.4. The number of the axial control volumes equals to that of the heat pipe. The root temperature of the fin is assumed to equal to the temperature of the pipe wall.

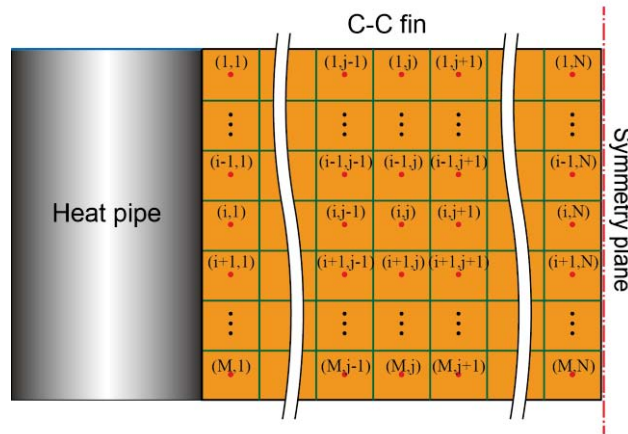


Fig. 4 Two-dimensional mesh of the fin

2.5. MATHEMATICAL MODEL OF THE TRANSPORT DUCT

The coolant collector in the middle of the radiator is designed with the two entrances and two exits. Just a quarter of it is taken to be analyzed for the symmetry. One-dimensional flow and heat transfer model is established. The control volume division is shown in Fig.5. To simplified the calculation, only ten heat pipes are modeled, and each one represents five adjacent heat pipes of the actual radiator.

In the process of calculation, The transport duct model obtains the coolant temperature and the convective heat transfer coefficient which will be considered as the evaporator boundary of the heat pipe. The heat pipe calculation will return the dissipation heat to the transport duct model as its inner heat source.

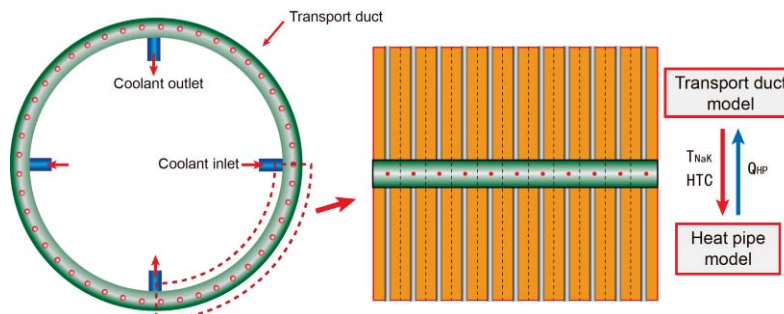


Fig. 5 The control volume division of the transport duct

3. RESULTS AND DISCUSSION

3.1. DESIGN PARAMETERS AND MATERIALS OF RADIATOR

The nominal thermal power of TOPAZ-II reactor is 115kW and the electric power is 5kW, so about 110kW waste heat should be rejected by the radiator. With reference to the similar radiator design, 200 heat pipes are selected and each one has a average power of 550W. The heat pipe design in this paper considered this single power as the design criteria. According to the operation requirements, the working fluid and structure materials are selected firstly. Then the geometric parameters are determined by the heat transfer limits. Table 1 shows the design values of the parameters.

Table I. Design parameters and materials of radiator components

Parameter	Value
Heat pipe	
Pipe wall material	Inconel
Porous wick material/type	Stainless Steel/ mesh
Working fluid	Potassium
Heat pipe total length/mm	600
Evaporator length/mm	100
Condenser length/mm	500
Radius of vapor space/mm	7.5
Wick average porosity	0.6
Wick thickness/mm	0.5
Pipe wall thickness/mm	1
Fin	
Fin material	Carbon-carbon
Fin Thickness/mm	0.4
Effective surface emissivity	0.9
Transport duct	
Wall material	Stainless steel
Length of cross section/mm	110
Width of cross section/mm	40
Diameter of the ring/mm	1800
Number of heat pipes	200

3.2. ANALYSIS OF THE RADIATOR UNDER NOMINAL CONDITION

Selected the first heat pipe in the calculation model to analyze in detail. From the temperature contour of the heat pipe shell and wick in Fig.6, we can see that the temperature in the outer part is higher than that of inner and the temperature difference between the out surface of the shell and inner surface of the wick is about 5K. In the condensing section, the inside temperature is higher than that of the outer part and the temperature difference is 0.7K. The difference between the temperature differences is caused by the length difference between the condenser and evaporator. Meanwhile, as shown in Fig.6, the condensing section has a good isothermal performance.

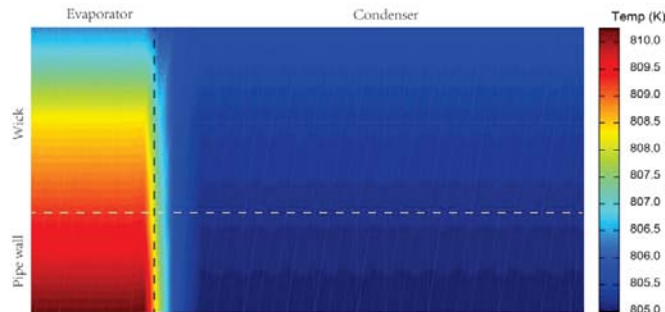


Fig. 6 Temperature distribution of the heat pipe wall and wick

Fig.7 shows the variation of the vapor parameters along the axial direction. It can be seen that the vapor pressure, temperature and density all reduce from evaporator to condenser. The vapor pressure drop of the whole length is 25Pa, the temperature difference is 0.6K and the density decreases by 0.2g/m^3 .

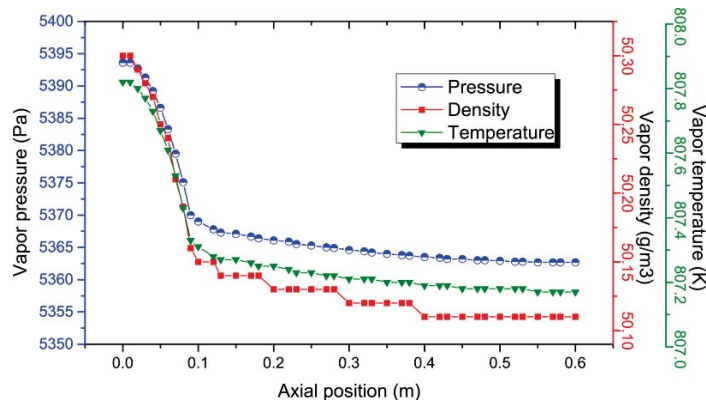


Fig. 7 Axial variation of vapor temperature, pressure and density

Fig.8 compares the temperature distributions of the heat pipe radiator fin and the coolant tube radiator fin. The left one is the former and the right one is the latter. Both are the hottest fins in the radiator calculation models. As we can see, the temperature of heat pipe radiator fin reduces in the direction vertical to the heat pipe and has a good isothermal performance in the longitude direction which is related to the constant temperature of the vapor. Meanwhile, the temperature difference between the maximum temperature and minimum temperature is also small. The maximum temperature is 792K while the minimum is 764K in this fin and the total temperature difference is just 28K. But from the temperature contour of the coolant tube radiator fin, we can see that it has a much larger temperature difference. The maximum temperature is 833K while the minimum is 735K and the total temperature difference is 98K. The reason is that the copper fin of the coolant tube radiator is in connection with the coolant tube which has a large temperature difference between the inlet and outlet. Therefore, for a single fin, the heat pipe radiator has a better isothermal performance and smaller thermal stress.

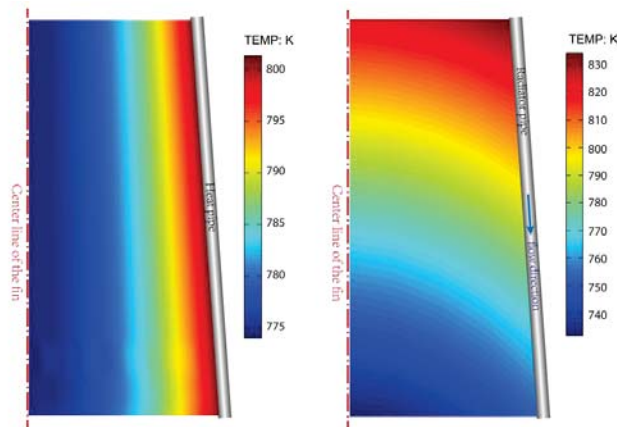


Fig. 8 Temperature distribution of the fin

Fig.9-11 are the results of a quarter of the radiator. Fig.9 shows the variation of average temperature of the coolant, evaporator and condenser along the coolant flow direction. The coolant temperature decreases from 843K to 744K which coincides with the TOPAZ-II design value. So the heat pipe radiator has the same heat dissipation ability as the coolant tube radiator under the nominal condition. It also can be seen that the main heat resistance locates between the coolant and the heat pipe outer surface. The maximum temperature difference between them is 20K(the coolant inlet side) and the minimum temperature difference is 13K(the coolant outlet side). The temperature difference between the evaporator and

condenser is just about 3K. Hence, the convection heat transfer enhancement between the coolant and the heat pipe is meaningful for increasing the capacity of the radiator.

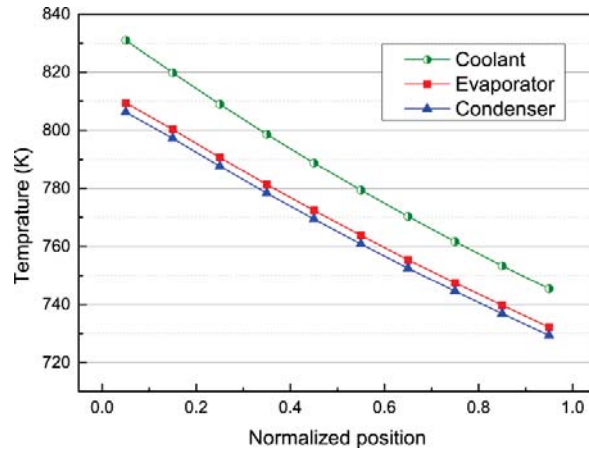


Fig. 9 Average temperature variation of the coolant, evaporator and condenser in the coolant flow direction

Fig.10 shows the variations of average temperature, pressure, density and velocity of the vapor along the transport duct. As we can see, the average temperature of the working fluid in different heat pipes decreases from 809K to 731K. The pressure and density also decrease with the temperature drop. But the velocities of the heat pipes increase along the transport duct. Although the powers of heat pipes reduce gradually in the coolant flow direction, but the lower temperature causes the reducing of the vapor density so that the vapor velocity becomes larger.

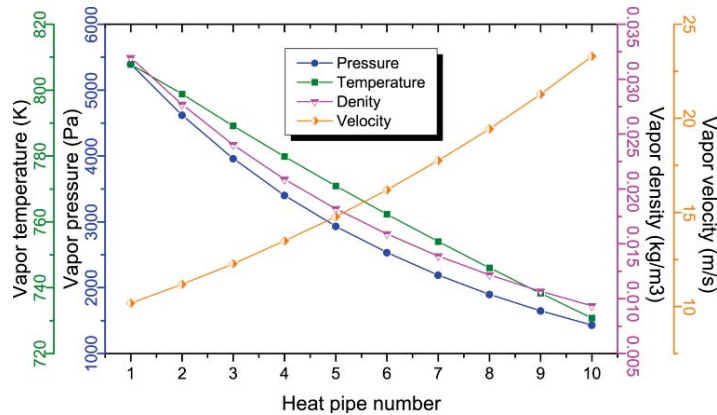


Fig. 10 Average temperature, pressure, density and velocity variations of vapor in the coolant flow direction

Fig.11 shows the axial variations of the vapor velocity of the selected five heat pipes. As we can see, the vapor velocity of the heat pipe near the coolant inlet is larger than that of the heat pipe in the other side. In each heat pipe, the vapor velocity increases from zero and then decreases to zero. In the evaporating section, the vapor accelerates due to the new vapor while in the condensing section the vapor slows down with the vapor condensing.

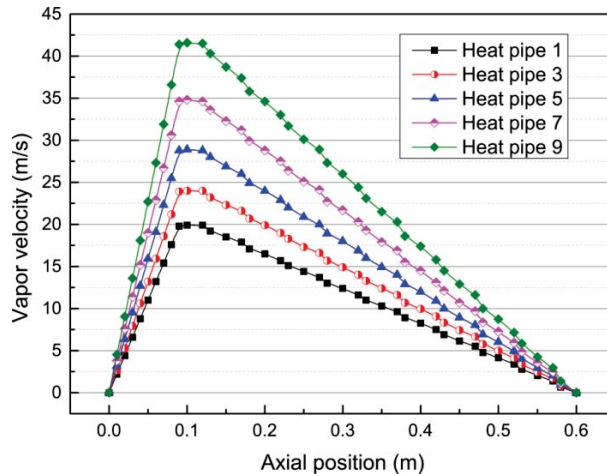


Fig. 11 Axial variations of vapor velocity of different heat pipes

3.3. ANALYSIS OF THE RADIATOR WITH DIFFERENT COOLANT INLET TEMPERATURE

Selecting five coolant inlet temperatures, 750K, 800K, 843K, 900K and 950K, the heat pipe radiator was calculated to analyse the heat rejection performance. Fig.12 shows the heat pipe power variation along the transport duct. As we can see, the power of heat pipe near the coolant inlet decreases from 1030W to 455W while that of the heat pipe near the outlet decreases from 629W to 331W. The thermal power of all the heat pipes fall by nearly half. Base on this, the coolant temperature has a great effect on the radiator power.

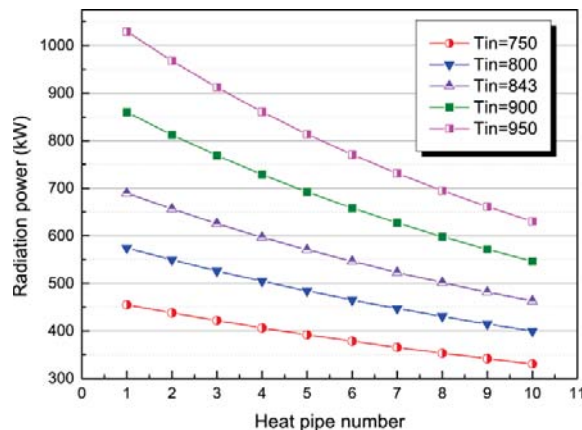


Fig. 12 Radiation power of the elements

The sonic, capillary and entrainment limits of the inlet potassium heat pipes are calculated at different coolant temperature, as shown in Fig.13. As we can see, the sonic limit is lowest in 750K, but it rises very fast with the increasing temperature and becomes much larger than the power of heat pipe. As a result, in high working temperature, the sonic limit has the smallest threats to the heat pipe operation. The capillary limit changes a little with the temperature and keeps at a low level. Therefore, when the heat pipe works at a high temperature, it would meet the capillary limit.

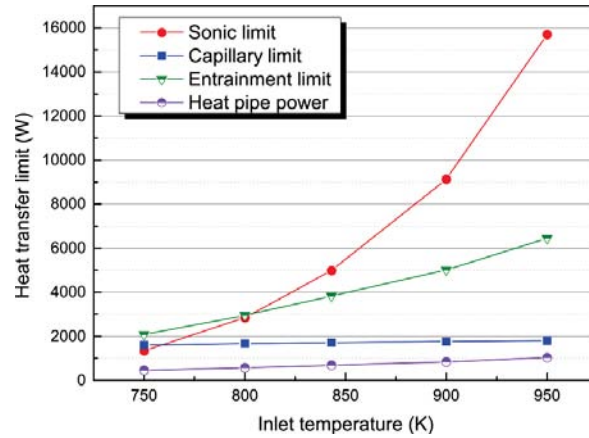


Fig. 13 Heat transfer limits

4. CONCLUSIONS

With reference to the design of similar radiators, a new heat pipe radiator is designed for the TOPAZ-II reactor power system in this paper to overcome the single point failure problem of the original coolant tube radiator and a steady-state numerical calculation was carried on to analyze the performance of this radiator. Some important conclusions can be summarized as follows:

- 1) The designed radiator can satisfy the heat rejection requirement of the TOPAZ-II under normal conditions and has a certain margin. The heat pipe radiator has a good isothermal performance and a smaller thermal stress.
- 2) The sonic limit of the heat pipe rises fast with the increasing temperature and the capillary limit changes a little with the temperature and keeps at a low level. The capillary limit has a greater harm on the heat pipe than the sonic limit, especially under a high working temperature.
- 3) The heat pipe radiator has a complex heat transfer process and several thermal resistances exist. The thermal resistance between the coolant and heat pipe wall is the largest.

NOMENCLATURE

Nomenclature			
Q	Heat power(W)	r	radius(m)
A	area(m ²)	l	length(m)
h	enthalpy(j.kg ⁻¹)	v	specific volume(m ³ .kg ⁻¹)
M	molecular weight (mol ⁻¹)	X	quality of vapor
T	temperature (K)	V	axial velocity (m.s ⁻¹)
d, D	diameter(m)	E	energy factor
p	pressure(Pa)	c	volumetric heat capacity(J.m ³ .K ⁻¹)
F	friction coefficient	f	view factor
m	mass	U	radial velocity (m.s ⁻¹)

Geek symbols

ρ	density(kg m ⁻³)	λ	heat conductivity(W.m ⁻¹ .K ⁻¹)
γ	specific heat ratio	ε	porosity
σ	Surface tension	θ	angle(°)

Stefan-Boltzmann constant

Subscripts

v	vapor	s	surrounding, wick, sonic
fg	fluid-gas	fin	fin
c	capillary	wc	welded fin
l	liquid	pw	pipe wall
g	Gravity, gas	sin	inner surface
e	entrainment	$sout$	outer surface
b	boiling	f	fluid

REFERENCES

1. Bennett G L, Hemler R J, Schock A. Space nuclear power-An overview[J]. Journal of propulsion and power, 1996, 12(5): 901-910.
2. Paramonov D V, El - Genk M S. A detailed thermal - hydraulic model of the TOPAZ - II radiator[C]//Proceedings of the 12th symposium on space nuclear power and propulsion: Conference on alternative power from space; Conference on accelerator - driven transmutation technologies and applications. AIP Publishing, 1995, 324(1): 485-493.
3. Von Arx A V. System simulation of a multicell thermionic space power reactor[M]. 1999.
4. EL-GENK M S, SEO J T. Study of the SP-100 radiator heat pipes response to external thermalexposure[J]. Journal of Propulsion and Power, 1990, 6(1): 69-77.
5. El-Genk M S, Tournier J M. DynMo-TE: Dynamic simulation model of space reactor power system with thermoelectric converters[J]. Nuclear engineering and design, 2006, 236(23): 2501-2529.
6. El-Genk M S, Tournier J M P. "SAIRS"—Scalable Amtec Integrated Reactor space power System[J]. Progress in Nuclear Energy, 2004, 45(1): 25-69.
7. El-Genk M, Tournier J M. Uses of Liquid-Metal and Water Heat Pipes in Space Reactor Power Systems[J]. Frontiers in Heat Pipes (FHP), 2011, 2(1).
8. Chen M M, Faghri A. An analysis of the vapor flow and the heat conduction through the liquid-wick and pipe wall in a heat pipe with single or multiple heat sources[J]. International journal of heat and mass transfer, 1990, 33(9): 1945-1955.